Graphene-bridged Multifunctional Flexible Fiber Supercapacitor with High Energy Density

Libo Gao [1,2,4], Jian Song [3,4], James Utama Surjadi [1], Ke Cao [1], Ying Han [1], Dong Sun Xiaoming Tao [3] and Yang Lu [1,2]

1 Department of Mechanical Engineering, City University of Hong Kong, Hong Kong SAR, Kowloon 999077, Hong Kong;

2 Shenzhen Research Institute, City University of Hong Kong, Shenzhen 518057, China;

3 Nanotechnology Center of Functional and Intelligent Textiles and Apparel Institute of Textiles and Clothing, The Hong Kong Polytechnic University, 999077, Hong Kong;

4 These authors contributed equally to this work.

5 E-Mail: yanglu@cityu.edu.hk ;

Abstract

Portable fiber supercapacitors with high energy storage capacity are in great demand to cater for the rapid development of flexible and deformable electronic devices. Hence, we employed a 3D cellular copper foam (CF) combined with the graphene sheets (GSs) as the support matrix to bridge the active material with nickel fiber (NF) current collector, significantly increasing surface area and decreasing the interface resistance. In comparison to the active material directly growing onto the NF in the absence of CF and GSs, our rationally designed architecture achieved a joint improvement in both capacity (0.217 mAh cm^{-2}/ 1729.413 mF cm^{-2}, 1200%enhancement) and rate capability (87.1% from 1 to 20 mA cm^{-2}, 286% improvement), which has never been achieved before with other fiber supercapacitors. in situ scanning electron microscope (SEM) micro compression test demonstrated its superior mechanical recoverability for the first time. Importantly, the assembled flexible and wearable device presented a superior energy density of 109.6 μWh cm^{-2} at a power density of 749.5 μW cm^{-2}, and successfully coupled with flexible strain sensor, solar cell and nanogenerator. This rational design should shed light on the manufacturing of 3D cellular architectures as micro current collectors to realize high energy density for fiber-based energy storage devices.

Keywords: *LDH; fiber s11percapacitor; mechanical recoverability; graphene; nano generator*

1. Introduction

The prosperity of portable electronics and smart textiles market stimulates the rapid evolution of flexible and wearable energy storage devices. [1-8] Fortunately, flexible fiber supercapacitor (FFSC) has shed light on the possibility of fabricating wearable energy electronics to meet this demand, where the first fiber-shaped energy storage device was fabricated by Baughman and coworkers using carbon nanotube fibers as electrodes.[9] Among them, metal fiber-based FSSC has recently aroused much attention because of high conductivity for charge transportation, which facilitates better electrochemical kinetics as well as superior mechanical strength compared to carbon based substrate.[3,10-12] However, the inferior areal energy density greatly limits its practical application considering that the usable area of an average human body or portable device is greatly limited.[13] Therefore, the key challenge in improving areal energy density lies in how to boost the areal capacity. However, many studies have focused on developing or updating new synthetic electrode materials to address this issue,[14,15] few works have focused on boosting the electrochemical performance only by optimizing the architecture of the electrode materials, current collector and the entire device without change the chemistry of the electrode materials. Structure design plays imperative role in guarantying the sufficient utilization and electrolyte ions accessing the inner part of the electrode materials.[15,16]

Considering the structural characteristics of metal fiber-based FSSC, the limited performance is likely due to the mean surface area for large-scale mass loading (areal capacity) and poor utilization of the electroactive-material (rate capability), both arising from its plain geometrical shape.[17,18] The construction of an intertwined 3D cellular architecture on a smooth substrate for depositing battery-type materials was able to alleviate this problem to a certain extent by allowing for increased surface area.[19,20] For instance, the bicontinuous porous Ni skeleton on nickel fiber (NF) or porous nickel wire as versatile hosts were fabricated to improve the electrochemical behavior.[21] In our previous works, we also have tried to address this issue through the inclusion of a rough surface carbon coating on smooth carbon fiber to enhance interface properties,[22] acid-assisted treatment in coarsening the nickel surface[23] and self-assembly of a highly conductive electro-active materials as porous "substrate" [24,25]. These architectures have proven that a 3D skeletal structure provides an effective way to enhance the surface area and mechanical adhesion of active material thus to achieve high areal capacity. Nevertheless, the intrinsic poor conductivity of battery-type electrode materials remains to limit its further applications. Additionally, based on Holm's theory, constriction/spreading resistance will be produced between electroactive materials and current collector because of the interface resistance generated by the two contacted electrodes, which is dependent on the amount of contact spots at the interface.[26] Consequently, decreasing the interface resistance of the electroactive material/ current collector remains to be a dilemma.

Due to the ultrahigh specific surface area and electrical conductivity, graphene sheets (GSs) have Jong been considered as an ideal candidate to act as electrode substrates, which allows the growth of battery-type materials through the formation of a conductive network for electron transportation and stress transfer.[27-32] For example, the vertically oriented graphene can bridge the active materials and planar current collector, which results in a significant increase in rate capability through the reduction of interfacial resistance originating from the limited contact points at the interface between the active layer and current collector.[29] Previous studies also show that NiCo LDH on GSs foam achieved ultrahigh areal capacitance and rate capability, demonstrating the possibility of using GSs as current collectors to relieve internal resistance.[27] Inspired by the aforementioned facts, the smart combination of a hierarchical 3D cellular graphene with battery-type electrode materials on metal wire would possibly not only enhance the surface area, but also lower the internal resistance to achieve high areal capacitance and rate capability. However, to our knowledge, it is lacking in research concerning this hypothesis to improve the energy delivery of FSSCs.

Here, we converted low-cost, wasted NF, cellular copper foam (CF) and graphene sheets (GSs) as well as layered double hydroxides (LDHs) into a FFSC with high areal capacity and rate capability. Through a series of electrodeposition (ED) and dip-coating operations, 3D cellular graphene framework was effectively cloned onto the NF. Notably, the CF was introduced as a scaffold to support the GSs while simultaneously acting as the micro current collector for electrons transportation. Such a double-sheath (CF and GSs) strategy allows a joint improvement in both areal capacity (0.217 mAh cm^{-2}/1729.4 mF cm^{-2}, 1200% enhancement) and rate capability (87.1% from 1 to 20 mA cm^{-2}, 286% increase) in contrast to growing the active materials directly onto a pristine NF. Importantly, the mechanical behavior of the composite was quantitatively studied for the first time using in situ scanning electron microscope (SEM). Finally, the as prepared wearable asymmetric FSSC with unprecedented energy density has been experimentally verified to be able to drive a series of electronic devices such as digital watch and calculator under typical bending deformation conditions. Furthermore, the rational integrations with a flexible strain sensor, piezoelectric-tribological nanogenerator, and flexible solar cell demonstrates its potential to be applied in a multitude of commercial and specialized electronic devices.

2. Results and discussions

Recycled NF was directly drawn from a wasted industrial nickel mesh (Figure 1a). After thorough cleaning, a glossy NF (400 μm in diameter) with smooth surface was obtained (Figure 1b and Figure 2a). Only featured peaks corresponding to nickel could be observed in the X-ray diffraction (XRD) spectrum, demonstrating the high purity of the

cleaned NF (Figure S1). Hydrogen templating routine is introduced in fabricating multiscale hierarchical porous CF which does not require the dissociation of a special sacrificial hard template. The ED process successfully converted the NF into CF-NF with kermesinus color within a short period of time (Figure 1c, d). SEM inspection (Figure 2c, d) revealed that the NF-CF inherited an ordered porous structure with pore sizes ranging from 20 to 50 μm and a layer thickness of approximately 50 μm after deposition for only 1 min at a constant current density of 1A cm^{-2}(the deposition time and current density can be optimized as shown in Figure S2). As a simple yet efficient route to "grow" GSs, dip-coating was extensively employed.[33,34] As shown in Figure 2e-f, the smooth GSs with an average thickness of below 40 nm (Figure S3) were homogeneously deposited onto the copper scaffold even at the innermost regions of the structure without aggregation. The corresponding characterization on graphene was shown in Figure S4. Specially, the XRD results (Figure S1) contain the pattern corresponding to graphite (002), indicating the multilayer and highly graphitic property of the GSs.[27] Although the real effect of multilayered GSs possibly is less than monolayer graphene, it is a promising candidate for electrode substrates.[35] Following the dip-coating process, a well-arranged and integrated composite NiCo LDH@GSs@CF-NF with porous architecture was successfully coated over the entire surface on NF (Figure2g and Figure S5) in comparison to that of the electrode materials directly growing on NF with exfoliation (Figure 2b). Simultaneously, numerous uniformly-distributed wrinkled and interconnected ultrathin NiCo LDH nanosheets with an open porous structure grew vertically and seamlessly on the GSs layer (Figure 2h) without any aggregation; XRD observations (Figure S1) further corroborated the presence of the LDH structure.[11] Therefore, several key requirements (high rate of electron transportation, large specific surface area, highly porous architecture and battery-type electrode materials) for improving capacitive performance were effectively merged together in the hierarchical composite structure. Thus far, there have been no reports of a FSSC which exhibited such hierarchically-ordered porous morphological features. The proposed design is expected to increase electrolyte accessibility through utilization of the inner active surface, consequently boosting the rate capability while providing a buffer for volumetric expansion during electrochemical reactions.

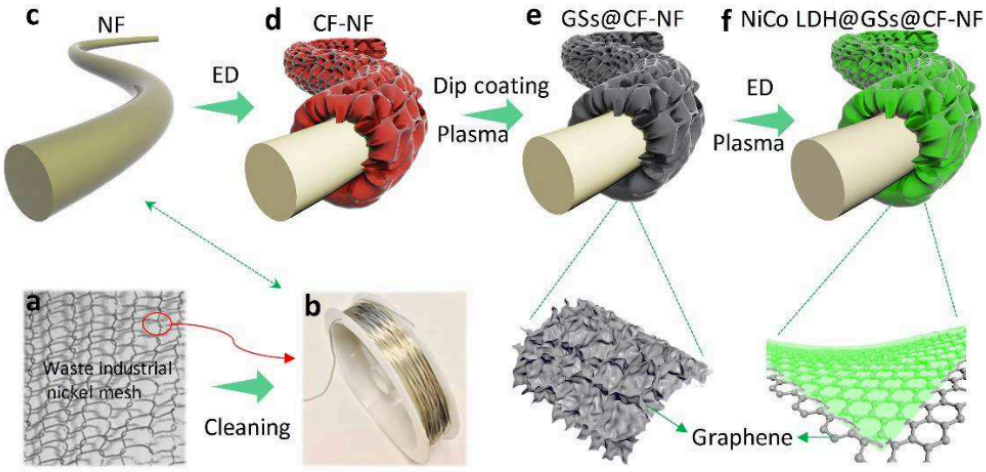

Figure 1. Schematic illustration of fabrication of the NiCo LDH@GSs@CF-NF using the industrial nickel mesh. (a-c) NF. (d) CF-NF. (e) GSs@CF-NF. (f) NiCo LDH@GSs@CF-NF.

Since GSs and NiCo LDH@GSs possess similar 20 micro-structures, the GSs serving as conductive backbones should have played a critical role in enhancing the mechanical loading capability of the WH. Various chemical and mechanical characterization methods were therefore employed to explore the mechanism involved. The typical transmission electron microscopy (TEM) images of the NiCo LDH@GSs in Figure 2i demonstrate the densely grown NiCo LDH on the copper skeleton (the dark part). Close-up observation of the composite in Figure 2i-j and Figure S6 unveiled that the ultrathin LDH sheet adheres well with the multilayer GSs. The lattice spacing in the higher resolution TEM (HRTEM, Figure 2k) observation was calculated to be 0.208nm, which agrees well with the (107) plane of the NiCo LDH.[36] Moreover, the element mapping analysis further confirms the homogeneous growth of NiCo-LDH on the GSs (Figure 21 and Figure S7).

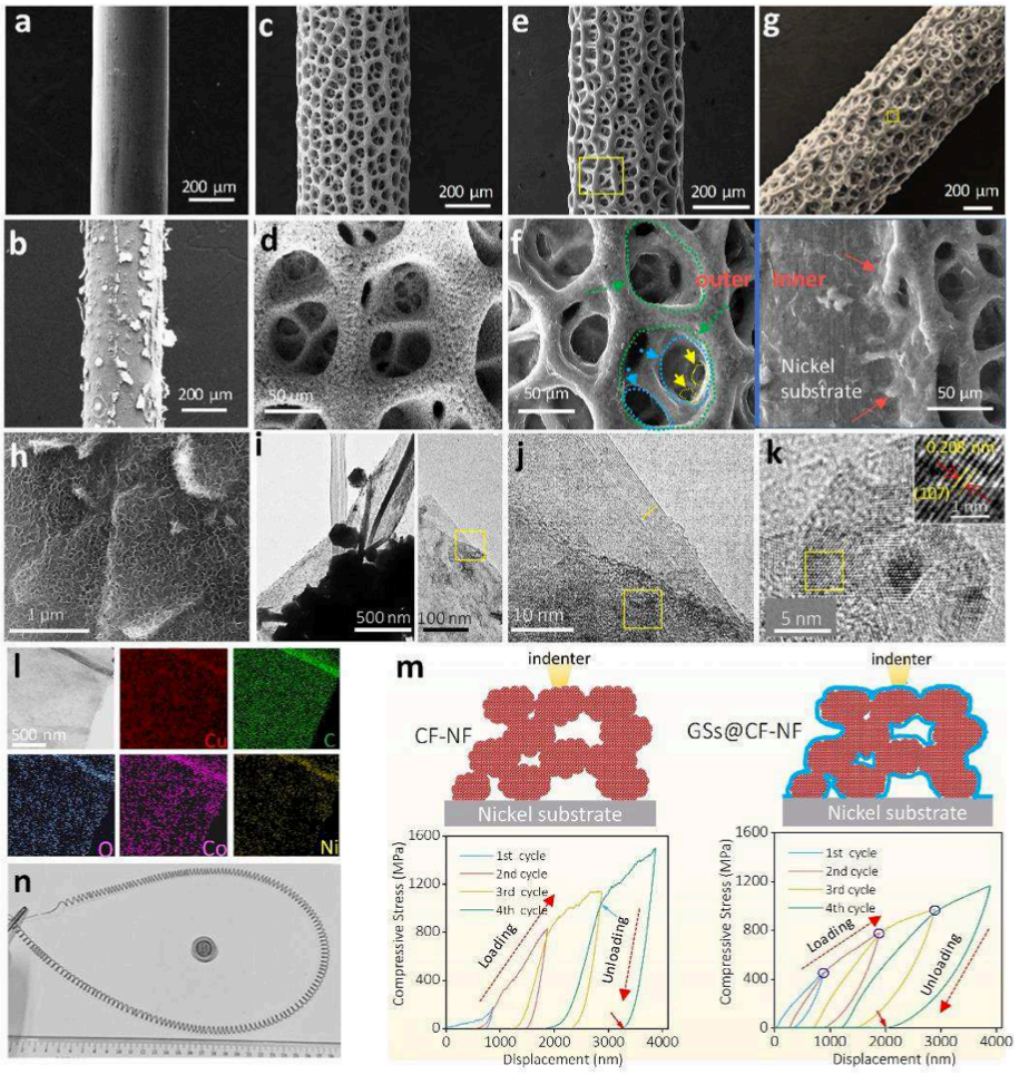

Figure 2. Structural and mechanical characterization of the NiCo LDH@GSs@CF-NF. SEM images of the (a) bare nickel wire and (b) NiCo LDH@NF. (c) low and (d) large view of the morphological features of CF-NF. (e) low and (f) large view of the morphological features of SEM images of the GSs@CF-NF. (g) SEM images of the NiCo LDH@GSs@CF-NF and (h) corresponding magnification. (i-k) low magnification and high resolution of TEM images of NiCo LDH@GSs@CF-NF. (l) Element mapping images and (m) micro-compression test of the GSs@CF-NF. (n) Large-scale fabrication of the GSs@CF- NF.

Figure 2m shows the schematic illustration of the compression test conducted on both the CF-NF and GSs/CF-NF (measured by *in situ* nanoindentation with a diamond indenter tip inside SEM, Figure S8a). The succeeding loading curve of the latter can almost completely go back to its previous maximum stress point and continue the trend of the previous loading curve over the entire range, indicating a nearly perfect strain memory effect.[37] However, the strain memory effect was not observed in the case for CF-NF, and each loading-unloading cycle exhibited an intermittent drop in force. Furthermore, we discovered that each cyclic compression on both samples would lead to a degree of permanent plastic deformation from the unloading curves, and the elastic recoverability of the GSs-coated one was 3.17 times of the CF-NF (red arrow, 2000 nm vs. 588 nm on recoverability) when subjected to 3867 nm compression. Considering the main difference between the two cases lies in the GSs coating, we propose that the energy

dissipation is mainly dependent on the buckling of the GSs which is tightly bounded to the CF, drastically elevating its structural integrity. This is verified by the post-mortem image shown in Figure S8b.The poor recoverability and intermittent force drop observed in the loading-unloading curves of the CF-NF is presumably attributed to the loosely stacked copper nanoparticles (Figure S8c-d). The weakly bonded nanoparticles would lead to limited electron transportation during the electrochemical reaction. Additionally, similar to other flexible fibers,[3,38] our GSs@CF-NF can also be readily rolled and curved into an arbitrary shape with a large scale production (Figure 2n). Consequently, these observations imply the uniform growth of a dense NiCo LDH layer on the substrate and the introduction of GSs would remarkably enhance the electrochemical performance, mechanical integrity and stability of the architecture when it suffered dynamic mechanical deformation, all of which plays a crucial role in practical applications.

The NiCo LDH@GSs@CF-NF composite exhibited superiority in electrochemical properties compared to all of its other controlled counterparts (Figure 3a), as indicated by the largest integrated areas of the cyclic voltammetry (CV) curves at *5* mV s^{-1} and the existence of two stronger reduction peaks (①②). A comparison of the galvanostatic charge-discharge curves (GCD) at I mA cm^{-2} further certify this observation (Figure 3b). The discharging time for NiCo LDH@GSs@CF-NF (781.3 s) is slightly larger than the NiCo LDH@CF-NF (685.8 s) but significantly exceeds NiCo LDH@NF (67.32 s) by more than I0 times. Apparently, the electrode materials could be sufficiently utilized with both the NiCo LDH@GSs@CF-NF and NiCo LDH@CF-NF at low current density. Whereas the NiCo LDH@NF displays the worst capacitive performance owing to the poor adhesion of NiCo LDH on the smooth NF (Figure 3b), leading to the low mass loading of the electrode material. It then naturally come to pose the question: where did the capacity of NiCo LDH@GSs@CF-NF mainly come from? Armed with above systematic analysis and considering that the capacity supplied by the pure nickel and GSs@CF-NF can almost be neglected (Figure S9 and Figure S10), the capacity is most likely to be derived from the battery-type capacitive reaction of the NiCo-LDH. Therefore, to have a better understanding of the corresponding capacitive performance, CV curves at various scan rates were quantitively shown in Figure S11a. The CV curves, especially at low scan rates, displayed two pairs of redox peaks. As the scan rate increases, the potential difference between the anode and cathode is attributed to the polarization of electrodes during the reaction process.[39] Figure S11b shows the GCD curves at different current densities ranging from 1 to 20 mA cm^{-2}. The linear variation of potential with time (0-0.16 V) alongside the vertical axis presented the double layer capacitance and the sloped variation of potential against time (0.16-0.45), which was attributed to the battery-type capacitive behavior arising from the redox activity,[40] further confirming the representative storage mechanism. However, to quantify the amount of charge stored by the battery-type reaction in the composite material, the CV curves obtained at various scan rates were fitted via using the kinetic models. The charge (Q, Cg^{-1}) and the scan rate

can be expressed according to the below equations.[41]

$$Q = Q_{v=\infty} + kv^{-1/2} \quad (1)$$

Or

$$Q^{-1} = Q_{v=0}^{-1} + kv^{1/2} \quad (2)$$

Where $Q_{v=\infty}$ represents the electric double layer charge (EDLC) when $v = \infty$. $Q_{v=0}$ stands the total charge when $v = 0$. Therefore, the total charge and the double layer charge can be calculated from the y-axis intercepts, as shown in Figure 3c-d. Based on the quantitative analysis, the diffusion-controlled redox capacitive contribution (Outer charge) is almost 90.2%, only 9.8% was derived from the inner charge (graphene layer). This result was in a good accordance with the observations displayed in Figure S9.

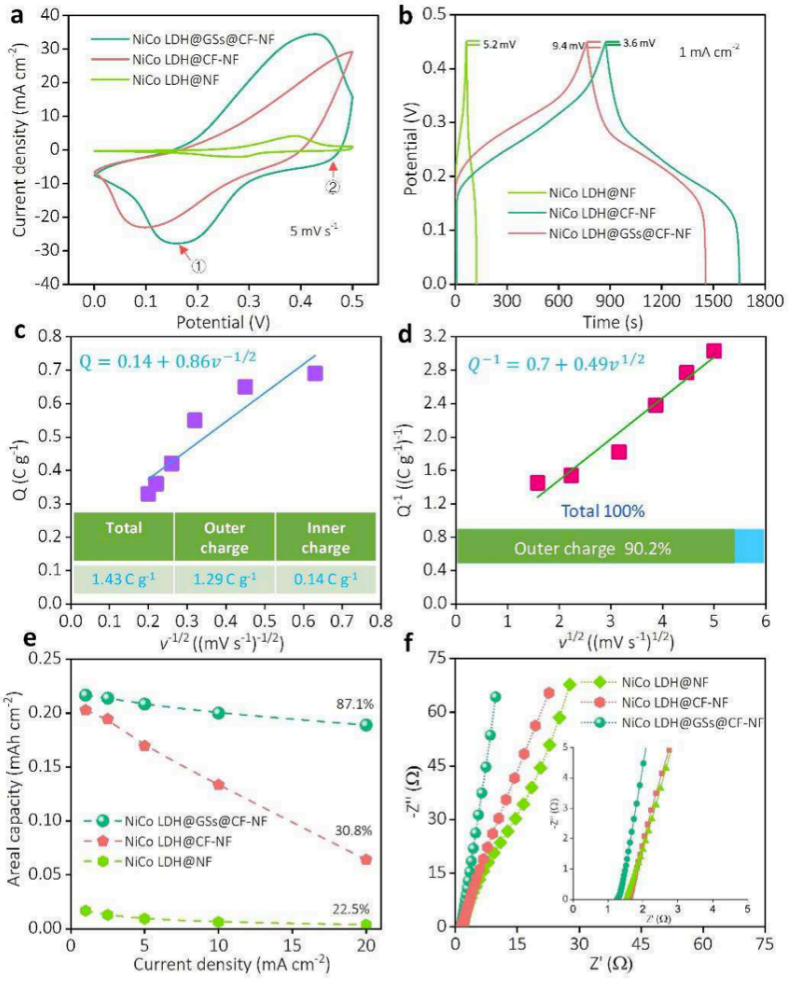

Figure 3. Electrochemical behavior of NiCo LDH@GSs@CF-NF. (a) CV curves, jk indicates the reduction peaks (b) GCD curves (c, d) relationships of charge vs. scan rate and (e) rate capability as well as (t) EIS measurement of NiCo LDH@GSs@CF-NF, NiCo LDH@CF-NF, and NiCo LDH@NF, respectively.

CF and GSs were two essential additives in the composites, understanding their respective roles in the electrochemical reaction are necessary to help us to decipher the mechanisms attributing towards the superior electrochemical performance. As studied above, at low current density, the NiCo LDH grown on CF-NF show larger capacity as opposed to direct deposition on a pristine NF. Based on this and SEM observations, we can schematically conclude: I) the 3D porous CF remarkably enhances the NiCo-LDH loading by avoiding delamination issues due to poor adhesion, non-uniformity, and constrained pores (Figure 2b); 2) the 3D porous architecture facilitates the diffusion of electrolyte ions into the inner regions of the electrode; 3) the large active area plays a crucial role in the enhancement of capacity. However, one remaining question is, in addition to the recoverable mechanical enhancement and "capacitive enhancement" for NiCo LDH@GSs@CF-NF at low current density (1 mA cm^{-2}), how does the GSs lead to increase the electrochemical performance? To address this doubt, rate capability tests were conducted to corroborate the role of the GSs. As shown in Figure 3e and Figure S12-S14, the NiCo LDH@GSs@CF-NF exhibits high areal capacity of 0.217, 0.214, 0.208, 0.2 and 0.189 mAh cm^{-2} (1729.4, 1714.7,1661.7,1599.7 and 1506.3 mF cm^{-2}) at current densities of 1, 2.5, *5,* 10,20 mA cm^{-2}, respectively. It achieved the highest areal capacity among the other fiber-shaped supercapacitors tested in an aqueous electrolyte and outperformed all of the previous reports which utilized a metal fiber as the substrate[8,21,42-45] (Table S1 in the Supporting information). For example, the 1729.4 mF cm^{-2} is almost two times higher than the recently reported 866 mF cm^{-2} at 2.5 mA cm^{-2} for CuO@CoFe LDH and three times higher than the $NiCo_2O_4$/3D nickel wire (550 mF cm^{-2}).[11,21] Moreover, the NiCo LDH@GSs@CF-NF achieved 6.8% and 1200% improvement in areal capacity compared to NiCo LDH@CF-NF (0.203 mAh cm^{-2}) and NiCo LDH@NF (0.017 mAh cm^{-2}) at a current density of 1 mA cm^{-2}. Surprisingly, the capacity of NiCo LDH@GSs@CF-NF remains to be 0.189 mAh cm^{-2} at current density of 20 mA cm^{-2}, achieving superior rate capability of 87.1% capacity retention whereas the NiCo LDH@CF-NF and NiCo LDH@NF only respectively kept 30.8% (0.063 mAh cm^{-2}) and 22.5% (0.0038 mAh cm^{-2}) capacity retention, respectively. Furthermore, this exceptional rate capability also exceeds all previously reported fiber supercapacitors such as NiO@CNT@CuO/Cu fiber (82.08% retention from 0.96 to 4.8 mA)[10] and NiO/$Ni(OH)_2$/PEDOT/Ni fiber (76.8% retention from 4 to 32 mA cm^{-2}).[46]

Cleary, the GSs are essential for the significant enhancement of rate capability. To analyze the rate capability mechanism of the composite, the *iR* drop (Figure 3b) was conducted on these samples. As a typical measure of the overall resistance of the electrode materials, the *iR* drop is proportional to discharge current.[47] As shown in Figure 3b, the NiCo LDH@Gs@CF-NF exhibits the lowest voltage drop (3.6 mV), indicating the smallest inner resistance. In contrast, the CF modification cannot improve the conductivity (as high as 9.4 mV) of the electrode, and its conductivity was even worse compared to the NiCo LDH@NF. This is attributed to the weak bonding of the copper nanoparticles discussed earlier. Therefore, we deemed that the introduction of GSs greatly eases the electrons resistance inside the electrode materials during the electrochemical reaction, due to its intrinsic high current-carrying ability deduced from the

hexagonal lattice structure (Figure Sl5).[48] The electrochemical impedance spectroscopy (EIS) was thus employed to further confirm and deeply probe it (Figure 3f). The nearly vertical curve for NiCo LDH@Gs@CF-NF in the low frequency indicates an ideal and perfect supercapacitor behavior. The largest slope of the profile for the graphene modified composite was derived from a fast ion diffusion process in the electrolyte, which stemmed from the GSs coating together with the rationally designed 3D porous copper structure. Conversely, the CF is inferior but higher than that of the NiCo LDH@NF, further demonstrating the role of 3D copper framework in enhancing the ions diffusion rate as a buffer reservoir. The series resistance (electrolyte resistance, intrinsic resistance and interfacial contact resistance) was defined as the intercept between the EIS and horizontal axis again validated the *iR* drop results (inset in Figure 3f). Based on aforementioned findings, we can schematically conclude the mechanisms behind the induced high rate capability by GSs was because of the establishment of a "super highway" for rapid transportation of electrons and ions resulting from the seamless connection between highly conductive GSs and NiCoLDH. This rationally designed architecture avoids severe aggregation, easing the pathways for hydrated ions to access the interior surfaces. However, note that long time deposition would lead to the over-dense packing and exfoliation of LDH in causing less expose of active sits, reducing the areal capacitance (Figure S16).[11] Finally, an excellent cycling stability with 86.7% was achieved after 5000 cycles at a scan rate of 50 mV s^{-1} (Figure S17), which is because that the readily porous structure of the electrode is capable of accommodating the volume change during cycling, leading to a longer lifespan.

However, it does not make any sense to say how good the electrodes are without practical applications. The most exciting improvement was the successful assembly of the NiCo LDH@GSs@CF-NF (as the positive electrode), activated carbon (AC) (as the negative electrode, see Figure S18 in Supporting information) and Polyvinyl Alcohol (PVA)/KOH into a high-performance solid asymmetrical supercapacitor (SASC) (Figure 4a and Figure S19). The heat shrinkable pipe was used to effectively avoid the electrolyte leakage and moisture contamination. As expected, the SASC works in a wide potential range of 0-1.5 V (Figure 4b and Figure S20), which greatly beyond the limits of the positive and negative electrodes individually, achieving a high energy density based on the typical formula:

$$E = \frac{1}{2}CV^2 \tag{3}$$

Where E is the power density, C is the specific capacitance and V is the voltage range. Since a larger potential (V) has been obtained, we urgently want to see how the SASC worked in terms of the capacitive performance. To unveil this doubt, the CV curves of the SASC at various scan rates ranging from 10 to 100 mV s^{-1} were shown in Figure 4c. A combination of both battery-type capacitor and double layered capacitor features was observed, without any distorted behavior with increasing the sweep rates, demonstrating an efficient ion transportation. The GCD curves in Figure 4d exhibit nearly linear and symmetric

behavior, further demonstrating the superior electrochemical reversibility. This was also proven by the coulombic efficiency results in Figure 4e. At a high current density of 20 mA cm^{-2}, higher coulombic efficiency of 98.99% was obtained, the occurrence of a fast and reversible electrochemical process at or near the electrode surface. Most importantly, the SASC show superior high areal capacitance of 350.9 mF cm^{-2} (52.1 F $g^{-1}$and 1949 mF cm^{-3}, see Figure S21) at a current density of 1 mA cm^{-2}. This greatly outperforms other reported fiber supercapacitors such as the VN/CNT//MnO_2/PEDOT/CNT (213.5 mF cm^{-2} at 0.3 mA cm^{-2})[49] and the CNT@ZnO@MnO_2//CNT (31.15 mF cm^{-2} at 10 μA)[50]. Thanks to the strong bonding force of the gel electrolyte and the shrinkable pipe compared to the aqueous electrolyte, the assembled device showed superior Jong-cycling stability of 90.5% after 3000 cycles (Figure 4f and Figure S22a), demonstrating its great potential in practical application in comparison with other reported fiber device such as Co_3Q_4//Graphene (84%,1000 cycles)[51], NiCoS//Graphene (86.2%,1000 cycles)[52]. Notably, our device achieved outstanding energy density of 109.6 μWh cm^{-2} (0.61 mWh cm^{-3}) at a power density of 749.5 μW cm^{-2} (4.17 mW cm^{-3}) and remained 64.2 μWh cm^{-2} even at a power density of 14997.6 μW cm^{-2} (Figure 4g). This value exceeds most of the reported fiber supercapacitors such as the MXene (Ti_3C_2Tx,7.3 μWh cm^{-2}, 132 μW cm^{-2})[53], MOF- templated CNTFs@$ZnCo_2Q_4$@Zn-Co-S (32.lμWh cm^{-2}, 698.2 μW cm^{-2})[54], NiCoS/nickel yam (48.7 μWh cm^{-2} , 553 μW cm^{-2})[52], MnO_2/PEDOT/CNT (96 μWh cm^{-2} , 270 μW cm^{-2})[49], CNT/carbon nanofiber (9.8 μWh cm^{-2}, 189.4 μW cm^{-2})[55], TiN@C nanotube (2.69 μWh cm^{-2} , 97 μW cm^{-2})[38],MnO_2/carbon fiber (1.428 μWh cm^{-2}, 51.4 μW cm^{-2})[56], MnO_2/gold wire (5.4 μWh cm^{-2} , 284 μW cm^{-2})[57], MnO_2/Graphene (11.9 μWh cm^{-2}, 400 μW cm^{-2})[58] and core-shell graphene fiber (0.17 μWh cm^{-2} , 100 μW cm^{-2})[59]. Furthermore, the ability of the solid fiber device to retain excellent performance even under various mechanical deformations is desirable to be used for flexible and wearable electronics. The inset in Figure 4h shows the digital optical images of the device with different bending degree from 0 to 180 degrees, who showed excellent overlapped GCD curves (Figure S22b) with only 5% decay (Figure 4h). This suggests the possibility of a direct integration of the device onto a flexible substrate to drive electronic devices or regarding it as the energy storage system, especially considering that the device show low leakage current and limited self-discharge (Figure S23). As a proof of concept, several real-life applications of the SASC were explored to demonstrate the feasibility of the device to be incorporated into wearable electronic devices.

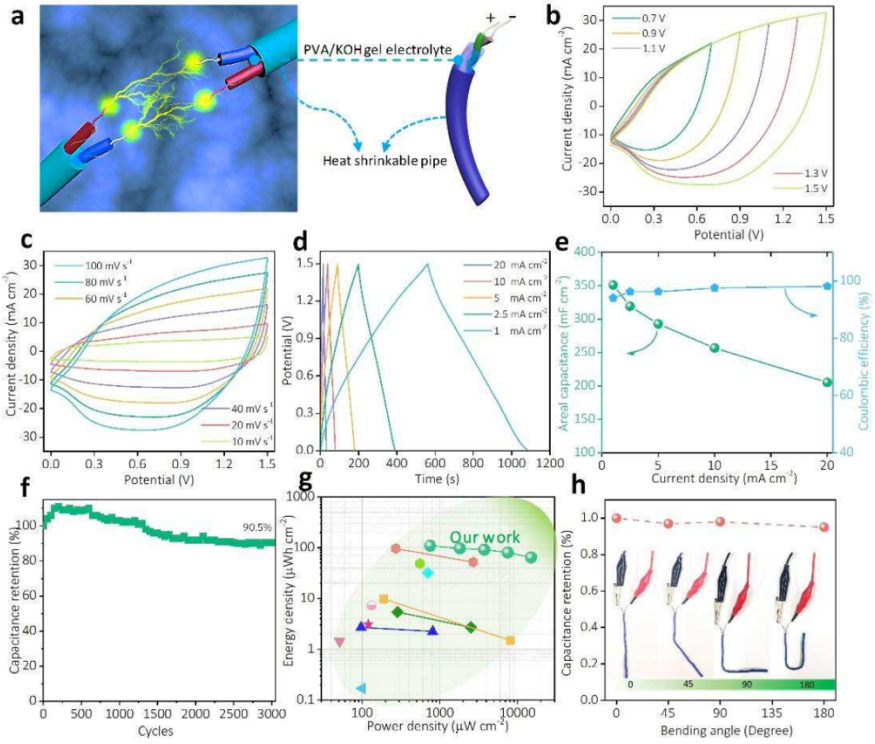

Figure 4. Electrochemical performance of the solid asymmetrical supercapacitor. (a) Schematic illustration of the assembled device. (b) Potential ranges of the SASC at a scan rate of 100 mVs^{-1}. (c) CV (d) GCD and (e) Rate capability as well as coulombic efficiency of the device. (f) Long-time cycling of the device. (g) Ragone plots of the device. (h) Capacitance retention of the device under various bending angles.

As shown in Figure S, the SASC was readily packaged with different devices, weaved into the cotton shirt and even flexed to fit our body shape. After charging for only 10 seconds, the curved individual SASC which was twined around a finger successfully powered a digital watch for more than 25 min (Figure 5a and Movie S1). The device was also integrated with a headphone, further demonstrating its capability to be worn and mold into our body shape (Figure 5b). Moreover, it could be weaved into our lab cloth to power electronics under bending deformation (Figure 5c, d). By employing several capacitors in series, the working potential can be increased accordingly to power devices which requires high energy density. As shown in Figure 5e-f, a motor fan and a pocket calculator can also be powered with the SASCs (Movie S2 and Movie S3).

Intriguingly, the device can be easily fixed on the magnetic paper without using extra force due to the ferromagnetic property of the nickel fiber,[60] further extending its functional applications (Figure S24).

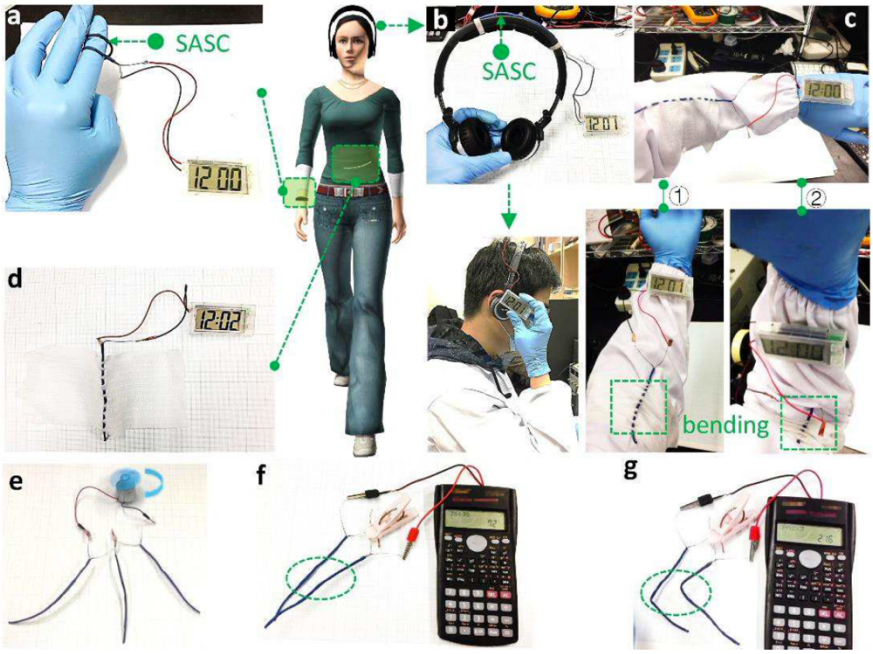

Figure 5. Practical application of the supercapacitor packaged with various electronic device. (a) The curved SASC powered a digital watch. (b) The device was integrated with a headphone. (c-d) the device was weaved into our lab cloth to power electronics under various bending deformation: ① (straight)② (bending). (e-g) a motor fan and a pocket calculator were powered with the SASCs.

Its potential to be used as a flexible strain sensor was also investigated by using an environmentally friendly and super-elastic yam obtained from disposable lab masks and coating it with rGO (Figure S25). The flexible SASC serves as the power source in this case as well (Figure 6a). Detailed fabrication procedures are included in the Supporting Information. The rationally designed strain sensor shows favorable gauge factor of 13.5 (Figure 6c), which is much higher than that of similar fabrics reported in Ref[61].Coherent with the demonstration shown in Figure 6c, the assembled device powered by the SASC exhibits high sensitivity and displayed oscillating electrical signal which is synchronized with the folding motion of the finger (Movie S4).

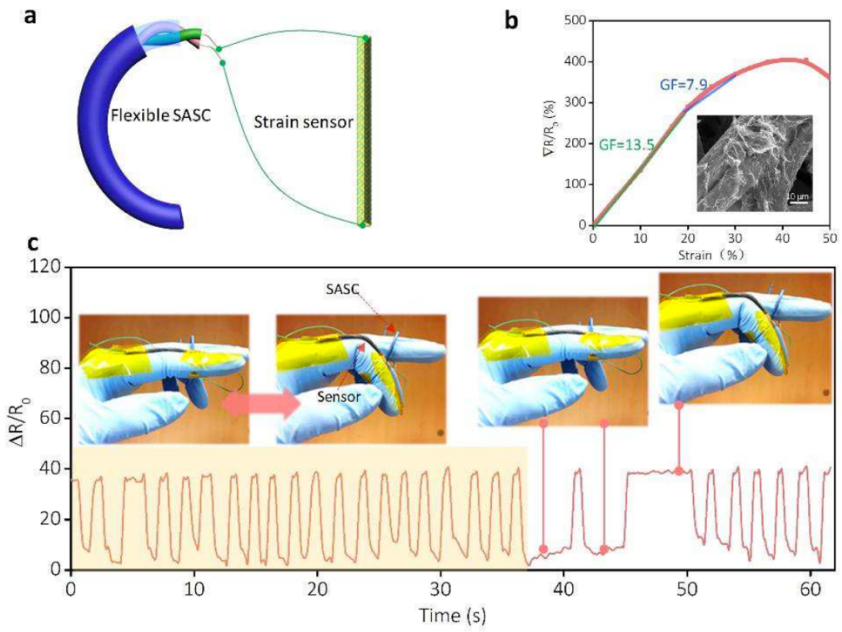

Figure 6. The device was assembled with a strain sensor. (a) The schematic illustration of the assembly. (b) The performance of the strain sensor. Inset is corresponding SEM images. (c) The behavior of the assembled SASC integrated with strain sensor.

The increasingly apparent energy crisis has forced people to find renewable and clean energy resources. However, due to the non-continuous and unstable nature resources (for example, the ocean wave owns a low frequency of below 5 Hz and the solar source is greatly limited by the geographical distribution, time shifting),[62,63] these nature energy sources typically cannot directly serve as the sole power source for driving consumer electronics. To tackle this problem, the supercapacitor can be regarded as the robust backup and reservoir to form a self-sustaining system. Thus, to demonstrate the viability of our device in storing ocean wave energy for practical application, the SASC was charged by the nanogenerator (piezoelectric and triboelectric units) with the frequency below 5 Hz (3 Hz, Figure 7a, and Figure S26). After charging for 30 min, the SASC (8 cm in length) increased its voltage from 0 to 90 mV, demonstrating its great potential in the storage of low frequency mechanical energy in our daily life (Figure 7b). Furthermore, the flexible SASC was readily packed with a bendable solar cell with a working voltage of 1.5 V under light to assemble a self-charging power system, as schematically illustrated in Figure 7c-d. Under the light irradiation, the SASC could not only drive the digital watch but also fully charge the SASC (Figure 7e). Thus, even when the light was removed (Figure 7f), the stored energy in the supercapacitor could serve as the power source for the watch, which enables this hybrid energy system to work for a prolonged period.

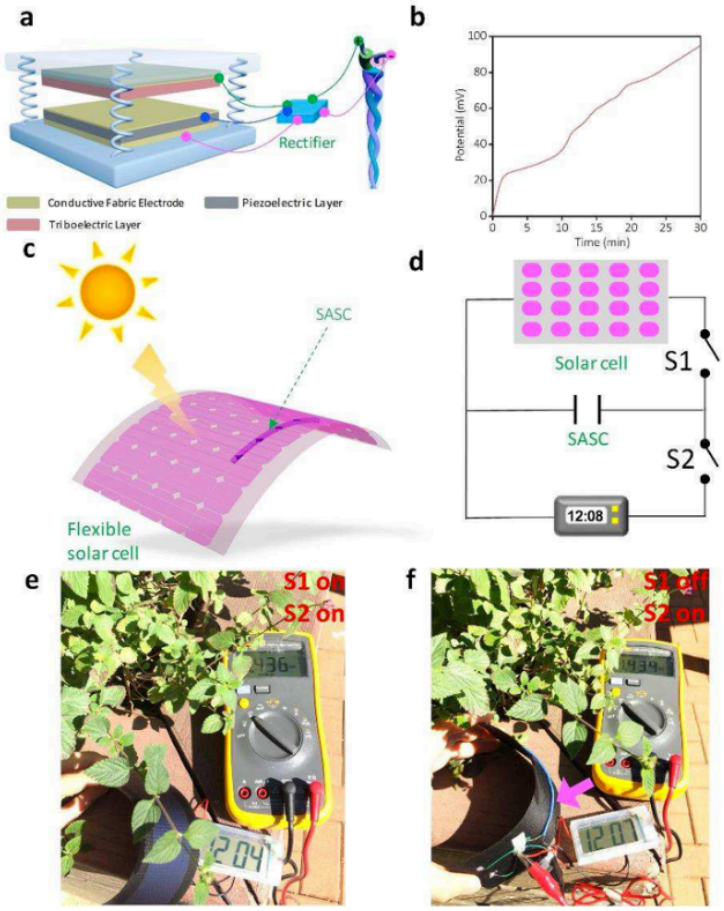

Figure 7. The SASC was packaged with nanogenerator and solar cell for energy storage. (a) Illustration of the assembled system (SASC with nanogenerator). (b) The charging curves as a function of the charging time. (c-f) The device was assembled with a flexible solar cell and corresponding digital optical images of the successful energy storage. Sl and S2 means the switch in the circuit.

3. Conclusions

To summarize, a rationally-designed strategy for the fabrication of FSSC with high energy density was proposed in this work. A 3D porous CF architecture was successfully built on NF for the first time, which not only act as a support for the graphene sheets but also served as the micro current collector, achieving high capacity. The GSs significantly lower the interfacial resistance and provide mechanical protection for the CF with superior recoverability to avoid catastrophic fracture (demonstrated by the *in situ* SEM compression test). Based on the cooperation between its constituents, the synthesized NiCo LDH@GSs@CF-NF exhibited 1200% improvement in areal capacity, 286% enhancement in rate capability and kept an excellent recycling ability. To our knowledge, such high areal capacity and rate capability rarely reported before. Importantly, the fabricated wearable FSSC could retain a high energy density even under mechanical deformation, allowing it to be readily integrated with other electronic devices to achieve multifunctional applications such as strain sensor, nanogenerator and flexible solar cell. Moreover, this

smart manufacturing strategy which utilized CF can be grafted to other metal wires (such as Cu wire, Ti wire and shape-memory alloy wire) and the method to coat GSs can be further optimized through chemical vapor deposition (CVD) to obtain a thinner graphene coating. This design principle creates new opportunities for developing fiber shaped energy storage device to achieve high energy output for applications in an extensive range of fields.

4. Experimental Section

Experimental procedure can be found in the Supporting information.

Supporting Information

Supporting information is available free of charge on the ACS Publications website at DOI:

Detailed experimental procedure; XRD patterns of the sample (Figure Sl); SEM and Raman test of the sample (Figure Sl-S7); in situ nanoindentation test of the graphene composite (Figure S8); Electrochemical performance of the NiCo LDH@GSs@CF-NF, NiCo LDH@CF-NF and NiCo LDH@NF (Figure S9-Sl4, Figure Sl6, Figure Sl7);

TEM images of the graphene sheets (Figure SI5); Electrochemical performance of the AC (Figure Sl8); Performance of the assembled device (Figure Sl9-S24); The performance of the strain sensor (Figure S25);The fiber supercapacitor was charged by the nanogenerator (Figure S26); Comparison of the fiber supercapacitor with other reported device (Table S 1); The curved individual SASC which was twined around a finger successfully powered a digital watch (Movie S1); A motor fan(Movie S2) and a pocket calculator(Movie S3) was powered with the SASCs; The strain sensor can be assembled with the SASC.

Author Information

Corresponding Author

*Email: yanglu@cityu.edu.hk

ORCID

Libo Gao: 0000-0002-5964-2337

Yang Lu: 0000-0002-9280-2718

Author Contributions

L.G. designed and conducted experiments, analyzed data, and wrote the main manuscript. J.S. conducted the experiments related with nanogenerator and wrote part of the manuscript. U.S.J. analyzed data and wrote part of the manuscript. K.C. performed the TEM experiments, and

Y.H. conducted the STEM-EDS of the samples. Y.L. supervised the research and revised the manuscript. All authors have given approval to the final version of the paper.

Notes

The authors declare no competing financial interest.

Acknowledgements

The authors wish to thank the Research Grants Council of the Hong Kong Special Administrative Region of China (GRF No. CityU 11216515) and City University of Hong Kong (Project Nos. 9667153 and 9680108). The authors also thank the funding supports from Shenzhen Science and Technology Innovation Committee under the grant JCYJ20170413141157573. Dong Sun acknowledges the funding from RGC under the project GRF CityU 11211714. Xiaoming Tao also thanks the PolyU152152/14E, PolyU15210/16E and PolyU152009/17E.

Reference

(1) Ren, J.;Bai,W.; Guan, G.; Zhang, Y .;Peng, H. Flexible and Weaveable Capacitor Wire Based on a Carbon Nanocomposite Fiber. *Adv. Mater.* 2013,*25,* 5965-5970.

(2) Fan, F. R.; Tian, Z. Q.; Lin Wang, Z. Flexible Triboelectric Generator. *Nano Energy* 2012, *1,*328-334.

(3) Xue, Y.; Ding, Y.; Niu, J.; Xia, Z.; Roy, A.; Chen, H.; Qu, J.; Wang, Z. L.; Dai, L. Rationally Designed Graphene-Nanotube 3D Architectures with a Seamless Nodal Junction for Efficient Energy Conversion and Storage. *Sci. Adv.* 2015, *1,* el400198.

(4) Lv, Z.; Luo, Y.; Tang, Y.; Wei, J.; Zhu, Z.; Zhou, X.; Li, W.; Zeng, Y.; Zhang, W.; Zhang, Y.; Qi, D.; Pan, S.; Loh, X. J.; Chen, X. Editable Supercapacitors with Customizable Stretchability Based on Mechanically Strengthened Ultralong Mn02 Nanowire Composite. *Adv. Mater.* 2018,*30,* 1704531.

(5) Sun, H.; Xie, S.; Li, Y.; Jiang, Y.; Sun, X.; Wang, B.; Peng, H. Large-Area Supercapacitor Textiles with Novel Hierarchical Conducting Structures. *Adv. Mater.* 2016, 28,8431-8438.

(6) Zhang, Y.;Yang, Y.;Gu, Y.;Yan,X.;Liao,Q.;Li, P.;Zhang,Z.;Wang,Z.Performance and Service Behavior in 1-DNanostructured Energy Conversion Devices. *Nano Energy* 2014, 14,30-48.

(7) Zhang, Z.; Xiao,F.; Qian,L.; Xiao,J.; Wang, S.;Liu, Y. Facile Synthesis of 3D Mn02- Graphene and Carbon Nanotube-Graphene Composite Networks for High-Performance, Flexible, All-Solid-State Asymmetric Supercapacitors. *Adv. Energy Mater.* 2014, *4,* 1400064.

(8) Zhang, Z.;Xiao, F.;Wang, *S.*Hierarchically Structured MnO 2 /Graphene/Carbon Fiber and Porous Graphene Hydrogel Wrapped Copper Wire for Fiber-Based Flexible All- Solid-State Asymmetric Supercapacitors. *J. Mater. Chem.A 2015*,*3,* 11215-11223.

(9) Dalton, A. B.; Collins,S.;Munoz, E.;Razal,J. M.;Ebron, V. H.; Ferraris,J. P.;Coleman, J. N.; Kim,B. G.; Baughman, R. H. Super-Tough Carbon-Nanotube Fibres. *Nature* 2003, *423,* 703.

(10) Nagaraju, G.; Sekhar, *S.* C.; Yu, J. *S.* Utilizing Waste Cable Wires for High- Perforrnance Fiber-Based Hybrid Supercapacitors: An Effective Approach to Electronic-Waste Management. *Adv. Energy Mater.* 2018, *8,* 1702201.

(11) Li,Z.;Shao, M.; Zhou, L.; Zhang, R.;Zhang, C.; Han, J.;Wei, M.; Evans, D. G.;Duan, X. A Flexible All-Solid-State Micro-Supercapacitor Based on Hierarchical CuO@layered Double Hydroxide Core-Shell Nanoarrays. *Nano Energy* 2016, *20,* 294- 304.

(12) Wen,J.;Li,S.;Zhou,K.;Song,Z.;Li, B.;Chen,Z.;Chen, T.;Guo, Y.;Fang,G. Flexible Coaxial-Type Fiber Solid-State Asymmetrical Supercapacitor Based on Ni3S2 Nanorod Array and Pen Ink Electrodes. *J. Power Sources* 2016,*324,* 325-333.

(13) Yang, Y.; Huang, Q.; Niu, L.; Wang, D.; Yan, C.; She, Y.; Zheng, Z. Waterproof, Ultrahigh Areal-Capacitance, Wearable Supercapacitor Fabrics. *Adv. Mater.* **2017,** *29,* 1606679.

(14) Chen, C.; Zhang, Y.; Li, Y.; Kuang, Y.; Song, J.; Luo, W.; Wang, Y.; Yao, Y.; Pastel, G.; Xie, J.; Hu, L. Highly Conductive, Lightweight, Low-Tortuosity Carbon Frameworks as Ultrathick 3D Current Collectors .*Adv. Energy Mater.* **2017,** 7, 1700595.

(15) Chen, C.; Zhang, Y.;Li, Y.;Dai,J.; Song,J.;Yao, Y.;Gong, Y.;Kierzewski, I.;Xie,J.; Hu ,L. All-Wood, Low Tortuosity, Aqueous, Biodegradable Supercapacitors with Ultra- High Capacitance. *Energy Environ.* Sci. **2017,** *JO,* 538-545.

(16) Sherrell, P. C.; Mattevi, C. Mesoscale Design of Multifunctional 3D Graphene Networks. *Mater. Today* **2016,** *19,*428-436.

(17) Meng, F.;Li,Q.;Zheng, L. Flexible Fiber-Shaped Supercapacitors: Design, Fabrication, and Multi-Functionalities. *Energy Storage Materials* 2017,8,85-109.

(18) Li,P.; Li,J .; Zhao, Z.; Fang, Z.; Yang, M.; Yuan, Z.;Zhang, Y.;Zhang, Q.; Hong, W.; Chen, X.; Yu, D. A General Electrode Design Strategy for Flexible Fiber Micro- Pseudocapacitors Combining Ultrahigh Energy and Power Delivery. *Adv.* Sci. **2017,** *4,* 1700003.

(19) Liu, L.; Zhao, H.; Wang, Y.; Fang, Y.; Xie, J.; Lei, Y. Evaluating the Role of Nanostructured Current Collectors in Energy Storage Capability of Supercapacitor Electrodes with Thick Electroactive Materials Layers. *Adv. Funct. Mater.* **2018 ,** *28,* 1705107.

(20) Zhang, Z.; Liu,*S.;* Xiao, J.; Wang, *S.* Fiber-Based Multifunctional Nickel Phosphide Electrodes for Flexible Energy Conversion and Storage. *J. Mater. Chem. A* **2016,** *4,* 9691-9699.

(21) Ramadoss, A.;Kang, K.-N.; Ahn, H.-J .; Kim, S.-1.; Ryu, S.-T.; Jang, J .-H. Realization of High Performance Flexible Wire Supercapacitors Based on 3-Dimensional NiCo20 4 /Ni Fibers. *J. Mater. Chem.A* **2016,** *4,*4718-4727.

(22) Gao, L.; Surjadi,J. U.; Cao, K.; Zhang, H.; Li,P.;Xu, *S.;* Jiang, C.;Song, J.; Sun, D.; Lu , Y. Flexible Fiber-Shaped Supercapacitor Based on Nickel-Cobalt Double Hydroxide and Pen Ink Electrodes on Metallized Carbon Fiber. *ACS Appl. Mater. interfaces* **2017,** *9,* 5409-5418.

(23) Gao, L.; Cao, K.; Zhang, H .; Li, P.; Song, J.; Surjadi, J. U.; Li, Y.; Sun, D.; Lu, Y. Rationally Designed Nickel Oxide Ravines@iron Cobalt-Hydroxides with Largely Enhanced Capacitive

Performance for Asymmetric Supercapacitors. *J. Mater. Chem. A* 2017, 5, 16944-16952.

(24) Gao,L.; ZHANG,H.;Surjadi,J. U.;Li, P.;Han , Y.;Sun,D.;Lu, Y. Mechanically Stable Ternary Heterogeneous Electrodes for Energy Storage and Conversion. *Nanoscale* **2018,** *JO,* 2613-2622.

(25) Yang, *S .;* Wu, C.;Cai, J.; Zhu, Y.;Zhang, H .; Lu, Y.;Zhang, K. Seed-Assisted Smart Construction of High Mass Loading Ni-Co-Mn Hydroxide Nanoflakes for Supercapacitor Applications. *J. Mater. Chem. A* **2017,** *5,* 16776--16785.

(26) Holm R. *Electric Contacts: Theory and Application; 4 th Ed;Springer:New York;* 1967.

(27) Xiong, G.; He, P.; Wang, D.; Zhang, Q.; Chen, T.; Fisher, T. *S.* Hierarchical Ni-Co Hydroxide Petals on Mechanically Robust Graphene Petal Foam for High-Energy Asymmetric Supercapacitors. *Adv. Funct. Mater.* 2016, *26,* 5460--5470.

(28) Zhao, M. Q.; Zhang, Q.; Huang, J. Q.; Wei, F. Hierarchical Nanocomposites Derived from Nanocarbons and Layered Double Hydroxides - Properties, Synthesis, and Applications. *Adv.Funct. Mater.* 2012, 22, 675--694.

(29) Bo,Z.;Zhu, W .;Ma, W.;Wen,Z.;Shuai, X .; Chen, J.; Yan, J .;Wang, Z.;Cen, K .;Feng, X. Vertically Oriented Graphene Bridging Active-Layer/Current-Collector Interface for Ultrahigh Rate Supercapacitors. *Adv.Mater.* 2013, *25,* 5799-5806.

(30) Zhang, Z.; Xiao, F.; Xiao, J.; Wang, S. Functionalized Carbonaceous Fibers for High Performance Flexible All-Solid-State Asymmetric Supercapacitors. *J.Mater. Chem. A 2015,3,* 11817-11823.

(31) Zhang, Z.; Chi, K.; Xiao, F.; Wang, S. Advanced Solid-State Asymmetric Supercapacitors Based on 3D Graphene/Mn02 and Graphene/Polypyrrole Hybrid Architectures. *J.Mater. Chem. A* 2015,*3,* 12828-12835.

(32) Zhang, Z.; Liu , M.; Tian, X.; Xu, P.; Fu, C.; Wang, S.; Liu, Y. Scalable Fabrication of Ultrathin Free-Standing Graphene Nanomesh Fi Lrns for Flexible Ultrafast Electrochemical Capacitors with AC Line-Filtering Performance. *Nano Energy* 2018, *50,* 182-191.

(33) Yu, G.; Hu, L.; Liu, N.; Wang, H.; Vosgueritchian, M .; Yang, Y. Enhancing the Supercapacitor Performance of Graphene/Mn02-Nanostructured Electrodes by Conductive Wrapping. *Nano Lett.* 2011, *11,*4438-4442.

(34) Jin, Y.; Chen, H.; Chen, M.; Liu, N.; Li, Q. Graphene-Patched CNT/Mn02 Nanocomposite Papers for the Electrode of High-Performance Flexible Asymmetric Supercapacitors. *ACS Appl .Mater. Interfaces* 2013,*5,*3408-3416.

(35) Song, Y.; Cai, X.; Xu, X.; Liu, X.-X. Integration of Nickel-cobalt Double Hydroxide Nanosheets and Polypyrrole Films with Functionalized Partially Exfoliated Graphite for Asymmetric Supercapacitors with Improved Rate Capability. *J. Mater. Chem. A* 2015, *3,* 14712-14720.

(36) Nagaraju, G.; Raju, G. S. R.; Ko, Y. H .; Yu, J. S. Hierarchical Ni-Co Layered Double Hydroxide Nanosheets Entrapped on Conductive Textile Fibers: A Cost-Effective and Flexible Electrode for High-Performance Pseudocapacitors. *Nanoscale* 2016, *8,* 812- 825.

(37) Yin, J .; Li, X.; Zhou, J .; Guo, W. Ultralight Three-Dimensional Boron Nitride Foam with Ultralow Permittivity and Superelasticity .*Nano Lett.* 2013, *13,*3232-3236.

(38) Sun, P.; Lin, R.;Wang, Z.;Qiu, M.;Chai, Z.; Zhang, B.;Meng, H.;Tan,S.;Zhao, C.; Mai, W. Rational Design of Carbon Shell Endows TiN@C Nanotube Based Fiber Supercapacitors with Significantly Enhanced Mechanical Stability and Electrochemical Performance. *Nano Energy 2011, 31,*432-440.

(39) Zhu, J.; Tang, S.; Wu, J .; Shi, X.; Zhu, B.; Meng, X. Wearable High-Performance Supercapacitors Based on Silver-Sputtered Textiles with FeCo2S4-NiCo2S4 Composite Nanotube-Built Multitripod Architectures as Advanced Flexible Electrodes. *Adv. Energy Mater.* 2017, 7, 1-11.

(40) Naveen, A. N.; Selladurai, S. Investigation on Physiochemical Properties of Mn Substituted Spine!Cobalt Oxide for Supercapacitor Applications. *Electrochim. Acta* 2014, 125, 404-414. Supercapacitor Using All-Carbon Material Electrodes. *ACS Nano* **2013,** 7, 5940-5947.

(41) Ardizzone, S.; Fregonara, G.;Trasatti, S. "Inner" and "Outer" Active Surface of Ru02 Electrodes.*Electrochim. Acta* 1990,*35,*263-267.

(42) Yang, H.; Xu, H.; Li, M.; Zhang, L.; Huang, Y.; Hu, X. Assembly of NiO/Ni(OH) 2/PEDOT Nanocomposites on Contra Wires for Fiber-Shaped Flexible Asymmetric Supercapacitors. *ACS Appl. Mater. Interfaces* 2016,*8,* 1774-1779.

(43) Dong, X.; Guo, Z.; Song, Y .; Hou, M.;Wang, J .; Wang, Y .;Xia, Y. Flexible and Wire- Shaped Micro-Supercapacitor Based on Ni(OH)2-Nanowire and Ordered Mesoporous Carbon Electrodes. *Adv. Funct. Mater.* 2014,*24,* 3405-3412.

(44) Huang, Y.; Hu, H.; Huang, Y.;Zhu, M.; Meng, W.;Liu,C.;Pei, Z.; Hao,C.; Wang,Z.; Zhi, C. From Industrially Weavable and Knittable Highly Conductive Yarns to Large Wearable Energy Storage Textiles. *ACS Nano* 2015, *9,*4766-4775.

(45) Fu, Y.; Cai, X.; Wu, H.; Lv, Z.; Hou, S.; Peng, M.; Yu, X.; Zou, D. Fiber Supercapacitors Utilizing Pen 1nk for Flexible/Wearable Energy Storage. *Adv. Mater.* 2012, 24, 5713-5718.

(46) Yang, H.; Xu, H.; Li, M.; Zhang, L.; Huang, Y.; Hu, X. Assembly of Ni0/Ni(OH)2/PEDOT Nanocomposites on Contra Wires for Fiber-Shaped Flexible Asymmetric Supercapacitors. *ACS Appl. Mater. Interfaces 2*016,*8,* 1774-1779.

(47) El-Kady, M. F.; Kaner, R. B. Scalable Fabrication of High-Power Graphene Micro-Supercapacitors for Flexible and on-Chip Energy Storage. *Nat. Commun.* 2013,*4,* 1475.

(48) Yu, J.; Liu, G.; Sumant, A. V.; Goyal, V.; Balandin, A. A. Graphene-on-Diamond Devices with Increased Current-Carrying Capacity: Carbon Sp2-on-Sp3 technology. *Nano Lett.* 2012, *12,* 1603-1608.

(49) Zhang, Q.; Wang, X.;Pan, Z.;Sun, J .;Zhao, J .;Zhang, J .; Zhang, C.;Tang, L.; Luo, J .; Song, B.; Zhang, Z.; Lu, W.; Li, Q.; Zhang, Y.; Yao, Y. Wrapping Aligned Carbon Nanotube Composite Sheets around Vanadium Nitride Nanowire Arrays for Asymmetric Coaxial Fiber-Shaped Supercapacitors with Ultrahigh Energy Density. *Nano Lett.* 2017, *17,*2719-2726.

(50) Li, Y.; Yan, X.; Zheng, X.;Si, H.;Li, M.; Liu, Y.; Sun, Y.;Jiang, Y.;Zhang, Y. Fiber- Shaped Asymmetric Supercapacitors with Ultrahigh Energy Density for Flexible/Wearable Energy

Storage. *J. Mater. Chem.A* 2016,4, 17704-17710.

(51) Wang, X.; Liu, B.; Liu, R.; Wang, Q.; Hou, X.; Chen, D.; Wang, R.; Shen, G. Fiber- Based Flexible All-Solid-State Asymmetric Supercapacitors for Integrated Photodetecting System. *Angew. Chemie Int. Ed.* 2014,*53,* 1849-1853.

(52) Chen, Y.; Xu, B.; Wen, J.; Gong, J.; Hua, T.; Kan, C.-W.; Deng, J. Design of Novel Wearable, Stretchable, and Waterproof Cable-Type Supercapacitors Based on High- Performance Nickel Cobalt Sulfide-Coated Etching-Annealed Yarn Electrodes. *Small 2018,14,* 1704373.

(53) Hu, M.; Li, Z.; Li, G.; Hu,T.;Zhang, C.;Wang, X. All-Solid-State Flexible Fiber-Based MXene Supercapacitors. *Adv. Mater. Technol.* 2017, 2, 1-6.

(54) Zhao,J.; Li,H.; Li, C.;Zhang, Q.;Sun,J.; Wang, X.; Guo, J.;Xie,L.; Xie, J.; He, B.; Zhou,Z.;Lu, C.;Lu, W.; Zhu,G.; Yao, Y.MOFfor Template-Directed Growth of Well- Oriented Nanowire Hybrid Arrays on Carbon Nanotube Fibers for Wearable Electronics Integrated with Triboelectric Nanogenerators. *Nano Energy* 2018,*45,*420-431.

(55) Le, V. T.; Kim, H.; Ghosh, A.; Kim, J.; Chang, J.; Vu, Q. A. Coaxial Fiber Supercapacitor Using All-Carbon Material Electrodes. ACS Nano 2013, 7, 5940-5947.

(56) Yu, N.; Yin, H.; Zhang, W.; Liu, Y.; Tang, Z.; Zhu, M. Q. High-Performance Fiber- Shaped All-Solid-State Asymmetric Supercapacitors Based on Ultrathin Mn02 Nanosheet/Carbon Fiber Cathodes for Wearable Electronics. *Adv.Energy Mater.* **2016,** *6,* 1-9.

(57) Xu, H.; Hu, X.; Sun, Y.; Yang, H.; Liu, X.; Huang, Y. Flexible Fiber-Shaped Supercapacitors Based on Hierarchically Nanostructured Composite Electrodes. Nano Res.2015,8, 1148-1158.

(58) Zheng,B.;Huang ,T.;Kou ,L.; Zhao,X.;Gopalsamy,K.;Gao,C. GrapheneFiber-Based Asymmetric Micro-Supercapacitors. J.Mater. Chem.A 2014, 2, 9736-9743.

(59) Meng, Y.;Zhao, Y .;Hu, C.;Cheng, H.;Hu, Y.;Zhang, Z.;Shi,G.; Qu, L.All-Graphene Core-Sheath Microfibers for All-Solid-State, Stretchable Fibriform Supercapacitors and Wearable Electronic Textiles.Ad v.Mater. 2013, 25, 2326--2331.

(60) Liu, Z.; Li, S.; Yang, Y.; Peng, S.; Hu, Z.; Qian, Y. Complex-Surfactant-Assisted Hydrothermal Route to Ferromagnetic Nickel Nanobelts. Adv. Mater. 2003, 15, 1946-1948.

(61) Du,D.; Li, P.; Ouyang, J. Graphene Coated Nonwoven Fabrics as Wearable Sensors. J. Mater. Chem. C 2016, 4,3224-3230.

(62) Xi, Y.;Guo, H.;Zi, Y.;Li, X.;Wang, J.;Deng,J.; Li,S.; Hu,C.; Cao,X.; Wang, Z. L. Multifunctional TENG for Blue Energy Scavenging and Self-Powered Wind -Speed Sensor. Adv. Energy Mater. 2017, 7, 1602397.

(63) Gao, Z.; Bumgardner, C.; Song, N.; Zhang, Y.; Li, J.; Li, X. Cotton-Textile-Enabled Flexible Self-Sustaining Power Packs via Roll-to-Roll Fabrication. Nat. Commun. 2016, 7, 11586.